Compilation of empirical and semi-empirical K_{α_1}, K_{α_2}, $K_{\beta'_1}$ and $K_{\beta'_2}$ X-ray fluorescence cross-sections by the application of Fitting approaches

K. Amari[1,2], A. Kahoul[1,2*], J.M. Sampaio[3,4], Y. Kasri[5,6], J.P. Marques[3,4], F. Parente[7], A. Hamidani[1,2], S. Croft[8], A. Favalli[9,10], S. Daoudi[1,2], A. Zidi[1,2], B. Berkani[1,2]

[1]*Department of Matter Sciences, Faculty of Sciences and Technology, Mohamed El Bachir El Ibrahimi University, Bordj-Bou-Arreridj 34030, Algeria.*
[2]*Laboratory of* Materials Physics, Radiation and *Nanostructures (LPMRN), Faculty of Sciences and Technology, Mohamed El Bachir El Ibrahimi University, Bordj-Bou-Arreridj 34030, Algeria.*
[3]*LIP – Laboratório de Instrumentação e Física Experimental de Partículas, Av. Prof. Gama Pinto 2, 1649-003 Lisboa, Portugal.*
[4]*Faculdade de Ciências da Universidade de Lisboa, Campo Grande, C8, 1749-016 Lisboa, Portugal.*
[5]*Department of Physics, Faculty of Sciences, University of Mohamed Boudiaf, 28000 M'sila, Algeria.*
[6]*Theoretical Physics Laboratory, Faculty of Exact Sciences, Bejaia University, 06000 Bejaia, Algeria,*
[7]*Laboratory of Instrumentation, Biomedical Engineering and Radiation Physics (LIBPhys-UNL), Department of Physics, NOVA School of Science and Technology, NOVA University Lisbon, 2829-516 Caparica, Portugal.*
[8]*School of Engineering, Faculty of Science of Technology, Nuclear Science, Engineering Research Group, Lancaster University, Bailrigg, Lancaster, LA1 4YW, United Kingdom.*
[9]*European Commission, Joint Research Centre, Ispra, I-21027, Italy.*
[10]*Los Alamos National Laboratory, P.O. Box 1663, Los Alamos, NM 87545, USA.*
[*]Corresponding author. Tel. /Fax (+213) 035862230.
E-mail address: a.kahoul@univ-bba.dz

Abstract:

In this study, empirical and semi-empirical X-ray fluorescence cross-sections were generated for K_{α_1}, K_{α_2}, $K_{\beta'_1}$ and $K_{\beta'_2}$ lines. The approach used was fitting of experimental data by three-dimensional formulae. The empirical values were computed through a fitting method including a three-dimensional function against atomic number Z and excitation energy E, resulting in a three-dimensional plot to estimate empirically a three-dimensional set of K_{α_1}, K_{α_2}, $K_{\beta'_1}$ and $K_{\beta'_2}$ X-ray fluorescence cross sections. Further, new semi-empirical values were derived by fitting the weighted average values using an analytical function against atomic number Z and the energy E and then the ratio $S_W = (\sigma_{K_i})_{Exp}/(\sigma_{K_i})_W$ are fitted by a three-dimension analyzed polynomial function according to atomic number Z and energy E. For K_{α_1} and K_{α_2} the range of atomic number covered was $52 \leq Z \leq 92$ whereas $K_{\beta'_1}$ and $K_{\beta'_2}$ it was $57 \leq Z \leq 79$. A comparison was made between our findings and selected experimental results, and good agreement was obtained.

Keywords: K-shell, XRF cross sections, empirical and semi-empirical calculation and fitting approaches.

1. Introduction

X-ray production cross-sections, intensity ratios, fluorescence yields, and vacancy transfer probabilities are atomic parameters needed across multiple application domains. Whether obtained through theoretical models, experimental investigation, or analytical techniques, they play a crucial role in diverse fields such as physical chemistry, medical research (including cancer treatment), X-ray analytical methods, radiation dosimetry, plasma characterization, radiation protection, and industrial radiation processing [1-4]. K-shell fluorescence cross-sections (K-XRFCSs) are frequently the most significant parameter and are essential to many different applications, including non-destructive testing and nuclear safeguards. The focus on this work was on the fluorescence cross-sections of K_{α_1}, K_{α_2}, $K_{\beta'_1}$ and $K_{\beta'_2}$ lines.

Our research group has made crucial contributions to the study of atomic parameters through a series of works on the empirical and semi-empirical calculation of various parameters, such as intensity ratios, fluorescence yields, Coster Kronig, vacancy transfer probabilities, as well as cross-sections under the effect of charged particles [5-13]. These studies have provided reliable results and significant advances in the field of atomic physics. However, A few studies have sought to compute K-shell fluorescence cross-sections across a broad range of elements at various excitation energies, utilizing either theoretical models or fitting experimental data using empirical and semi-empirical Formulae. For example, Krause *et al.* [14] compiled a theoretical table of K-XRFCSs along with useful formulae and essential parameters for calculating these cross-sections. Puri *et al.* [15] gives a less exhaustive table but claims to offer updated data of K-shell ($13 \leq Z \leq 92$) and L-shell series for ($35 \leq Z \leq 92$) XRFCS across incident photon energy range 1-200 keV. Kup Aylikci *et al.* [16] have investigated experimental and semi-empirical K_α and K_β XRFCSs for $_{27}$Co and $_{30}$Zn at 59.5 keV. Doğan *et al.* [17] examined experimental and semi-empirical analyses of the K_α and K_β XRFCSs for the same elements

using 59.5 keV gamma-rays. Besides, measured, empirical, and semi-empirical K-XRF cross-sections within atomic span $21 \leq Z \leq 30$ excited by photon of 59.5 keV have analyzed by Aylikci *et al*. [18]. Further, Kup Aylikci *et al.* [19] calculated measured and semi-empirical σ_{K_α} and σ_{K_β} production cross-sections of $_{26}$Fe and $_{30}$Zn at 59.5 keV. Subsequently, in 2018, Kup Aylikci *et al.* [20] performed semi-empirical K-shell X-ray fluorescence cross-sections and average fluorescence yields for sulfur compounds at 59.5 keV. Afterward, in 2019, the semi-empirical determinations of $K_{\alpha_{1,2}}, K_{\beta_{1,3}}$ and $K_{\beta_{2,4}}$ X-ray natura line widths for various elements between $29 \leq Z \leq 74$ at 123.6 keV was authored by Kup Aylikci *et al.* [21]. Finally, our group published empirical and semi-empirical calculations of K_α, K_β and K_{tot} X-ray fluorescence cross-sections for photons ranging from5.46 keV to 123.6 keV using three-dimensional formulas in Amari *et al.* [22,23].

This investigation involves providing the empirical and semi-empirical computations of X-ray fluorescence cross-sections for K_{α_1} and K_{α_2} $(52 \leq Z \leq 92)$, $K_{\beta'_1}$ and $K_{\beta'_2}$ $(57 \leq Z \leq 79)$ lines for whole photon energy based on fitting available experimental values published recently by our research team using three-dimensional analytical functions.

2. Empirical and semi-empirical computational methodologies

Two papers on the empirical and semi-empirical computation of K_α, K_β and K_{tot} X-ray fluorescence cross-sections for elements in the atomic range $16 \leq Z \leq 92$ for photon energies spanning the interval from 5.46 to 123.6 keV using three-dimensional formulas have recently been published by Amari *et al.* [22,23]. We have adopted this method here to estimate K_{α_1}, K_{α_2} , $K_{\beta'_1}$ and $K_{\beta'_2}$ XRFCSs. Our motivation was to use these empirical and semi-empirical approaches to gain a deeper insight into K X-ray fluorescence cross-sections and to support the generation of missing data points for various elements. Our fits rely on the availability of an extensive experimental data assembled and reported by our research team [24] for K_{α_1} and

K_{α_2} $(52 \leq Z \leq 92)$, $K_{\beta'_1}$ and $K_{\beta'_2}$ $(57 \leq Z \leq 79)$ at various energies. The attraction of the approach is that it does not rely on direct use of complex theoretical models, while allowing the relationships between atomic parameters and cross-sections to be captured in a simple yet precise manner.

2.1. Empirical technique

We firstly plotted the collected set of reliable experimental values for K_{α_1}, K_{α_2} , $K_{\beta'_1}$ and $K_{\beta'_2}$ as a function of atomic number Z and energy E. Following that, we fitted these experimental data. Notably, the analytical function utilized for the fitting process is as follows:

$$(\sigma_X)_{Emp} = g(Z,E) \times P(Z) \qquad \text{with } X = K_{\alpha_1}, K_{\alpha_2}, K_{\beta'_1} \text{ and } K_{\beta'_2} \tag{1}$$

where,

$g(Z,E) = c.Z^5.E^{-d}$ and P (Z) is a simple third-degree polynomial given as:

$$P(Z) = \sum_n a_n Z^n = a_0 + a_1 Z + a_2 Z^2 + a_3 Z^3 \tag{2}$$

One can thing of $g(Z,E)$ as describing the main functional dependence which emerges from basic theoretical analysis, and P (Z) as an empirical data driven modification function to capture the realistic physical behaviors. The fitting coefficients c, d and a_n are summarized in Table 1. The results of fitting are depicted in Fig.s 1-4 by a surface.

2.2. Semi-empirical method

Motivated by our previous work on the study of semi-empirical XRF cross-sections using a three-dimensional analytical function [23], in this investigation, we propose to apply the same approach to fit the weighted average values for K_{α_1}, K_{α_2} , $K_{\beta'_1}$ and $K_{\beta'_2}$ XRFCSs. To begin, we graphed the quantity $(\sigma_X)_W$ against atomic number Z and energy E. Afterward, an analytical function was utilized to model these data, as detailed below:

$$(\sigma_X)_W = H(Z,E) \times Q(Z) \qquad \text{with } X = K_{\alpha_1}, K_{\alpha_2}, K_{\beta'_1} \text{ and } K_{\beta'_2} \tag{3}$$

Hence,

$H(Z,E) = k.Z^5.E^{-\gamma}$, and Q (Z) is a simple third-degree polynomial described as:

$$Q(Z) = \sum_n m_n Z^n = m_0 + m_1 Z + m_2 Z^2 + m_3 Z^3 \tag{4}$$

The findings of the fitting are represented by a surface in Fig. s 5-8.

Subsequently, we plotted the ratios S according to atomic number Z and energy E as shown in Fig. s 9-12. Furthermore, we applied an analytical function to fit the data, as outlined below:

$$S = \frac{\left(\sigma_{K_i}\right)_{Exp}}{\left(\sigma_{K_i}\right)_W} = f(Z) \times R(E) \tag{5}$$

where,

f(Z) is a second-order polynomial and R(E) is a third-degree polynomial expressed as:

$$f(Z) = \sum_i b_i Z^i = b_0 + b_1 Z + b_2 Z^2 \tag{6}$$

$$R(E) = \sum_j l_j E^j = l_0 + l_1 E + l_2 E^2 + l_3 E^3 \tag{7}$$

From Eq. s (3) and (5) we define the semi-empirical cross-sections as:

$$(\sigma_X)_{Sem-emp} = (\sigma_X)_W \times S \qquad \text{with } X = K_{\alpha_1}, K_{\alpha_2}, K_{\beta'_1} \text{ and } K_{\beta'_2} \tag{8}$$

The fitting parameters for both Eq. s (3) and (5) are listed in Table 2.

To determine the fitting coefficients for Eq. s (1) and (8), we employed a fitting process. This fitting technique was executed using version 5.4 patchlevel 8 of Gnuplot software, an open-source plotting tool managed by a team of volunteers, utilizing the provided fitting functions. After obtaining the fitted parameters, we visualized the data points and the fitting functions

using Origin 2021 software, which is a data analysis and graphing tool developed by OriginLab Corporation, Northampton, MA, USA.

The total deviation of the experimental cross-sections from the corresponding fitted values is expressed in terms of the root-mean-square error ($\varepsilon_{\mathrm{rms}}$). It is calculated for each K_x line ($x = \alpha_1, \alpha_2,\ \beta'_1$ and β'_2) using the following expression:

$$\varepsilon_{\mathrm{rms}} = \left[\sum_{i=1}^{N} \frac{1}{N}\left(\frac{(\sigma_{\mathrm{K}x})_{exp} - (\sigma_{\mathrm{K}x})_{S-emp/emp}}{(\sigma_{\mathrm{K}x})_{S-emp/emp}}\right)^2\right]^{1/2} \quad (9)$$

where N is the number of data points.

3. Results and discussion

Tables 3-6 provides, respectively, a summary of present empirical and semi-empirical K_{α_1} and K_{α_2} $(52 \leq Z \leq 92)$, $K_{\beta'_1}$ and $K_{\beta'_2}(57 \leq Z \leq 79)$ X-ray fluorescence cross-sections for photon energies ranging from 59.5 keV to 123.6 keV. For each K_x line ($x = \alpha_1, \alpha_2,\ \beta'_1$ and β'_2) the total root-mean-squares error ($\varepsilon_{\mathrm{rms}}$) of the empirical and semi-empirical results is also displayed in Tables 1 and 2. A comparison was conducted between the empirical and semi-empirical cross-sections deduced from Eq. s (1) and (8) along with experimental cross-sections reported by [25-27] for K_{α_1} and K_{α_2} $(52 \leq Z \leq 92)$ at 123.6 keV and those of Akman et al. [28] for $K_{\beta'_1}$ and $K_{\beta'_2}(57 \leq Z \leq 79)$ at 59.5 keV to evaluate the accuracy of fitting methods. The results of this comparison are highlighted in Fig. s 13-16. Reviewing these figures allows us to make several comments:

It can be seen from Fig. s 15 and 16 that for $K_{\beta'_1}$ and $K_{\beta'_2}$ that the experimental results of Akman *et al.* [28] are in good agreement with both the empirical and semi-empirical calculations derived from Eq. s (1) and (8). Besides, for $K_{\beta'_1}$ the deviation (D (%)) between the current empirical cross-sections and those of Akman *et al.* [28] vary in the range of 0.72-6.19%, also

the deviation between our semi-empirical cross-sections and the experimental values of Akman *et al.* [28] ranging from 1.27% to 6.70% for a whole atomic range.

For $K_{\beta'_2}$, the measured values of Akman *et al.* [28] agrees within the error range of 0.42-13.01% and 0.67-13.51% with the empirical values estimated from Eq (1) and semi-empirical values established from Eq (8), respectively.

For K_{α_1}, a strong correlation is observed between the empirical data derived from formula (1) and the experimental values of Kaya *et al.* [25] within 7-18.18% for elements $_{52}$Te, $_{56}$Ba, $_{60}$Nd, $_{64}$Gd, $_{68}$Er, $_{72}$Hf and $_{74}$W, Ertuğral *et al.* [26] within 11.82-19.81% for elements with $59 \leq Z \leq 64$ except for $_{58}$Ce the deviation is about 24.13%, and Apaydın and Tıraşoğlu [27] within 0.49-16.48% for elements with atomic numbers $65 \leq Z \leq 92$ except for $_{75}$Re the deviation is 21.08%. Furthermore, our semi-empirical results exhibit an acceptable range of concordance, with deviations ranging from 5.05% to 18.60% except for $_{59}$Pr (24.02%) for Ertuğral *et al.* [26] and from 0.53% to 14.43%, except for $_{92}$U (21.77%) and $_{75}$Re (22.26%) for Apaydın and Tıraşoğlu [27]. In contrast, the comparison reveals disagreement between our semi-empirical findings and the experimental values of Kaya *et al.* [25] with a variation span from 18.71% to 96.04%.

Fig. 14 depicts a high consistency between K_{α_2} X-ray empirical results described by the formula (1) and those obtained experimentally [25-27] with D vary in the range of 1.46-17.49% for Kaya *et al.* [25], 0.28-10.01% for Ertuğral *et al.* [26], 0.47-19.05% for Apaydın and Tıraşoğlu [27]. Moreover, the current semi-empirical values align closely with the experimental values of Kaya *et al.* [25] with D extends from 5.55% to 12.35%. Additionally, semi-empirical values match well with the measured data of Ertuğral *et al.* [26] with variations in the range of 0.74%-10.83%. Subsequently, the semi-empirical computations fall well with the experimental values reported by Apaydın and Tıraşoğlu [27] while some inconsistencies are noted for elements with

$65 \leq Z \leq 69$. Within the error range of these calculations, the deviation varies from 0.47% to 15.45% for elements with $70 \leq Z \leq 92$, and in the range of 21.76% - 24.93% for targets with atomic numbers $65 \leq Z \leq 69$.

We highlight that the formula used to calculate the deviations between our results and other experimental values is

$$\mathrm{D}\ (\%) = \left|\frac{(\sigma_{\mathrm{K}_i})_{exp} - (\sigma_{\mathrm{K}_i})_X}{(\sigma_{\mathrm{K}_i})_X}\right| \times 100 \quad \text{with } (i = \alpha_1, \alpha_2,\ \beta'_1 \text{and } \beta'_2 \text{hence } X = emp\ or\ S-emp) \tag{10}$$

4. Conclusion

This study focused on the computations of empirical and semi-empirical K_{α_1} and K_{α_2} ($52 \leq Z \leq 92$), $K_{\beta'_1}$ and $K_{\beta'_2}$ ($57 \leq Z \leq 79$) X-ray fluorescence cross-sections for photons of 59.5 keV, 78.706 keV, 121.9 keV, and 123.6 keV. Furthermore, our results deduced from Eq. s (1) and (8) were compared to other experimental results. In general, the findings of this comparison show a good agreement with the experimental measurements. Moreover, these results provide valuable insights into the accuracy of empirical and semi-empirical models for describing X-ray fluorescence cross-sections. Although, the differences seen at Z-values and specific photon energies indicate the necessity for more extensive experimental data for elements with medium to heavy weights. Enhancing precision in measurements at energy levels could help refine the empirical and semi-empirical models more effectively. This study provides a massive data and a reliable archive for researchers in the field of radiation detection and atomic physics.

Acknowledgments

We gratefully acknowledge the support of the DGRSDT, Ministry of Higher Education and Scientific Research, Algeria. This work was done with the support of Mohamed El Bachir El Ibrahimi University, under project (PRFU) N°: B00L02UN340120230003. This work was also supported by the Fundação para a Ciência e Tecnologia (FCT), Portugal through contracts UIDP/50007/2020 (LIP) and UID/FIS/04559/2020 (LIBPhys). S.C. warmly acknowledges the financial support of Lancaster University, and A.F. gratefully acknowledges the support of the Joint Research Centre of the European Commission.

Figures captions

Fig. 1. The distribution of the experimental K_{α_1} XRFCS as a function of atomic number *Z* and photon energy for 59.5, 78.706, 121.9 and 123.6 keV. The fitting result is also presented as a surface.

Fig. 2. The distribution of the experimental K_{α_2} XRFCS as a function of atomic number *Z* and photon energy for 59.5, 78.706, 121.9 and 123.6 keV. The fitting result is also presented as a surface.

Fig. 3. The distribution of the experimental $K_{\beta'_1}$ XRFCS as a function of atomic number *Z* and photon energy for 59.5, 78.706 and 123.6 keV. The fitting result is also presented as a surface.

Fig. 4. The distribution of the experimental $K_{\beta'_2}$ XRFCS as a function of atomic number *Z* and photon energy for 59.5, 78.706 and 123.6 keV. The fitting result is also presented as a surface.

Fig. 5. The distribution of the weighted average $(\sigma_{K_{\alpha_1}})_W$ XRFCS values against atomic number *Z* and photon energy for 59.5, 78.706, 121.9 and 123.6 keV. The fits are also represented by a surface.

Fig. 6. The distribution of the weighted average $(\sigma_{K_{\alpha_2}})_W$ XRFCS values against atomic number *Z* and photon energy for 59.5, 78.706, 121.9 and 123.6 keV. The fits are also represented by a surface.

Fig. 7. The distribution of the weighted average $(\sigma_{K_{\beta'_1}})_W$ XRFCS values against atomic number *Z* and photon energy for 59.5, 78.706 and 123.6 keV. The fits are also shown by a surface.

Fig. 8. The distribution of the weighted average $(\sigma_{K_{\beta'_2}})_W$ XRFCS values against atomic number Z and photon energy for 59.5, 78.706 and 123.6 keV. The fits are also shown by a surface.

Fig. 9. The distribution of the ratio $S = (\sigma_{K_{\alpha_1}})_{Exp}/(\sigma_{K_{\alpha_1}})_W$ according to the atomic number Z and photon energy for 59.5, 78.706, 121.9 and 123.6 keV. The fits are also represented by a surface.

Fig. 10. The distribution of the ratio $S = (\sigma_{K_{\alpha_2}})_{Exp}/(\sigma_{K_{\alpha_2}})_W$ according to the atomic number Z and photon energy for 59.5, 78.706, 121.9 and 123.6 keV. The fits are also represented by a surface.

Fig. 11. The distribution of the ratio $S = (\sigma_{K_{\beta'_1}})_{Exp}/(\sigma_{K_{\beta'_1}})_W$ according to the atomic number Z and photon energy for 59.5, 78.706 and 123.6 keV. The fits are also shown by a surface.

Fig. 12. The distribution of the ratio $S = (\sigma_{K_{\beta'_2}})_{Exp}/(\sigma_{K_{\beta'_2}})_W$ according to the atomic number Z and photon energy for 59.5, 78.706 and 123.6 keV. The fits are also shown by a surface.

Fig. 13. The empirical $(\sigma_{K_{\alpha_1}})_{emp}$ and semi-empirical $(\sigma_{K_{\alpha_1}})_{S-emp}$ XRFCSs compared to the experimental findings of [25-27] as a function of atomic number Z at a photon energy of 123.6 keV.

Fig. 14. The empirical $(\sigma_{K_{\alpha_2}})_{emp}$ and semi-empirical $(\sigma_{K_{\alpha_2}})_{S-emp}$ XRFCSs compared to the experimental findings of [25-27] as a function of atomic number Z at a photon energy of 123.6 keV.

Fig. 15. The empirical $(\sigma_{K_{\beta'_1}})_{emp}$ and semi-empirical $(\sigma_{K_{\beta'_1}})_{S-emp}$ XRFCSs compared to the experimental findings of [28] as a function of atomic number Z at photon energy of 59.5 keV.

Fig. 16. The empirical $(\sigma_{K_{\beta'_2}})_{emp}$ and semi-empirical $(\sigma_{K_{\beta'_2}})_{S-emp}$ XRFCSs compared to the experimental findings of [28] as a function of atomic number Z at photon energy of 59.5 keV.

References

[1] Scofield, J. H., California Univ., Livermore. Lawrence Livermore Lab. No. UCRL-51326 (1973).

[2] Hubbell, J. H. and Seltzer, S. M., National Institute of Standards and Technology, Gaithersburg, MD. No NIST IR 5632 (1995).

[3] Berger, M. J., Hubbell, J. H., Seltzer, S. M. and Chang, J., J. Appl. Phys. 58(10) 2333-2342 (2010).

[4] Hakcley, M. S., Springer Science and Business Media. (2011).

[5] Aylikci, V., Kahoul, A., Kup Aylikci, N., Tiraşoğlu, E., Karahan, İ. H., Abassi, A. and Dogan, M. Radiat. Phys. Chem. 106, 99-125 (2015).

[6] Khalfallah, F., Deghfel, B., Kahoul, A., Aylikci, V., Kup Aylikci, N. and Nekkab, M. Radiat. Phys. Chem. 112, 71-75 (2015)

[7] Derradj, I., Kahoul, A., Deghfel, B., Bendjedi, A., Khelfallah, F., Sahnoune, Y., Bentabet, A. and Nekkab, M. Radiat. Phys. Chem. 121, 81-86 (2016).

[8] Berkani, B., Kahoul, A., Sampaio, J. M., Daoudi, S., Marques, J. P., Parente, F., Hamidani, A., Croft, S., Favalli, A., Kasri, Y., Zidi, A. and Amari, K. Radiat. Phys. Chem. 225, 112106 (2024)

[9] Aylikci, V., Kahoul, A., Kup Aylikci, N., Tiraşoğlu, E. and Karahan, İ. Spectrosc. Lett. 48, 331-342 (2015).

[10] Kup Aylikci, N., Sampaio, J. M., Kahoul, A., Aylikci, V., Karahan, I. H., Guerra, M., Santos, J. P., Marques, J. P. and Tiraşoğlu, E. X-Ray. Spectrom. 46, 242-251 (2017).

[11] Zidi, A., Kahoul, A., Marques, J. P., Daoudi, S., Sampaio, J. M., Parente, F., Hamidani, A., Croft, S., Favalli, A., Kasri, Y., Amari, K. And Berkani, B. J. Electron Spectros. Relat. Phenomena. 275, 147473 (2024).

[12] Meddouh, K., Daoudi, S., Kahoul, A., Sampaio, J. M., Marques, J. P., Parente, F., Kup Aylikci, N., Aylikci, A., Kasri, Y. and Hamidani, A. Radiat. Phys. Chem. 202, 110481 (2023).

[13] Hamidani, A., Daoudi, S., Kahoul, A., Sampaio, J. M., Marques, J. P., Parente, F., A., Croft, S., Favalli, A., Kup Aylikci, N., Aylikci, A., Kasri, Y. and Meddouh, K. At. Data Nucl. Data Tables. 149, 101549 (2023).

[14] Krause, M. O., Nestor, C. W. Jr., Sparks, C. J. Jr. and Ricci, E., Oak. Ridge. National. Lab. No. ORNL-5399, 7032250 (1978).

[15] Puri, S., Chand, B., Mehta, D., Garg, M. L., Singh, N. and Trehan, P. N., At. Data Nucl. Data Tables. 61, 289–311 (1995).

[16] Kup Aylikci, N., Aylikci, V., Kahoul, A., Tiraşoğlu, E., Karahan, İ. H. and Cengiz, E., Phys. Rev. A. 84 042509 (2011).

[17] Dogan, M., Tirasoglu, E., Karahan, İ. H., Kup Aylikci, N., Aylikci, V., Kahoul, A., Cetinkara, H. A. and Serifoglu, O., Radiat. Phys. Chem. 87, 6–15 (2013).

[18] Aylikci, V., Kahoul, A., Aylikci, N. K., Tiraşoğlu, E. and Karahan, İ. H., Spectrosc. Lett. 48, 331–342 (2015).

[19] Kup Aylikci, N., Sampaio, J. M., Kahoul, A., Aylikci, V., Karahan, I. H., Guerra, M., Santos, J. P., Marques, J. P. and Tiraşoğlu, E., X-Ray Spectrom. 46, 242–251 (2017).

[20] Kup Aylikci, N., Sancak, K., Aylikci, V., Tirasoglu, E., Unluer, D., Depci, T., Chem. Phys. Lett. 706, 40–46 (2018.).

[21] Kup Aylikci, N., Spectrosc. Lett. 52, 346–355 (2019).

[22] Amari, K., Kahoul, A., Sampaio, J. M., Kasri, Y., Marques, J. P., Parente, F., Hamidani, A., Croft, S., Favalli, A., Daoudi, S., Deghfel, B., Zidi, A. and Berkani, B., 2024 Phys. Scr. 99 105402 (2024).

[23] Amari *et al* , xxxxxxxxx.

[24] Amari, K., Kahoul, A., Sampaio, J. M., Daoudi, S., Marques, J. P., Parente, F., Hamidani, A., Croft, S., Favalli, A., Kasri, Y., Zidi, A. and rBerkani, B., At. Data Nucl. Data Tables. 159 101662 (2024).

[25] Kaya, N., Apaydin, G., Tirasoglu, E., Chem. 80, 677–681 (2011).

[26] Ertuğral, B., Eur. Phys. J. D 44, 313–317 (2007).

[27] Apaydın, G., Tıraşoğlu, E., Nucl. Instrum. Methods Phys. Res. Sect. B Beam Interact. Mater. At. 246, 303–308 (2006).

[28] Akman, F., Appl. Radiat. Isot. 115, 295–303 (2016).

Fig. 1

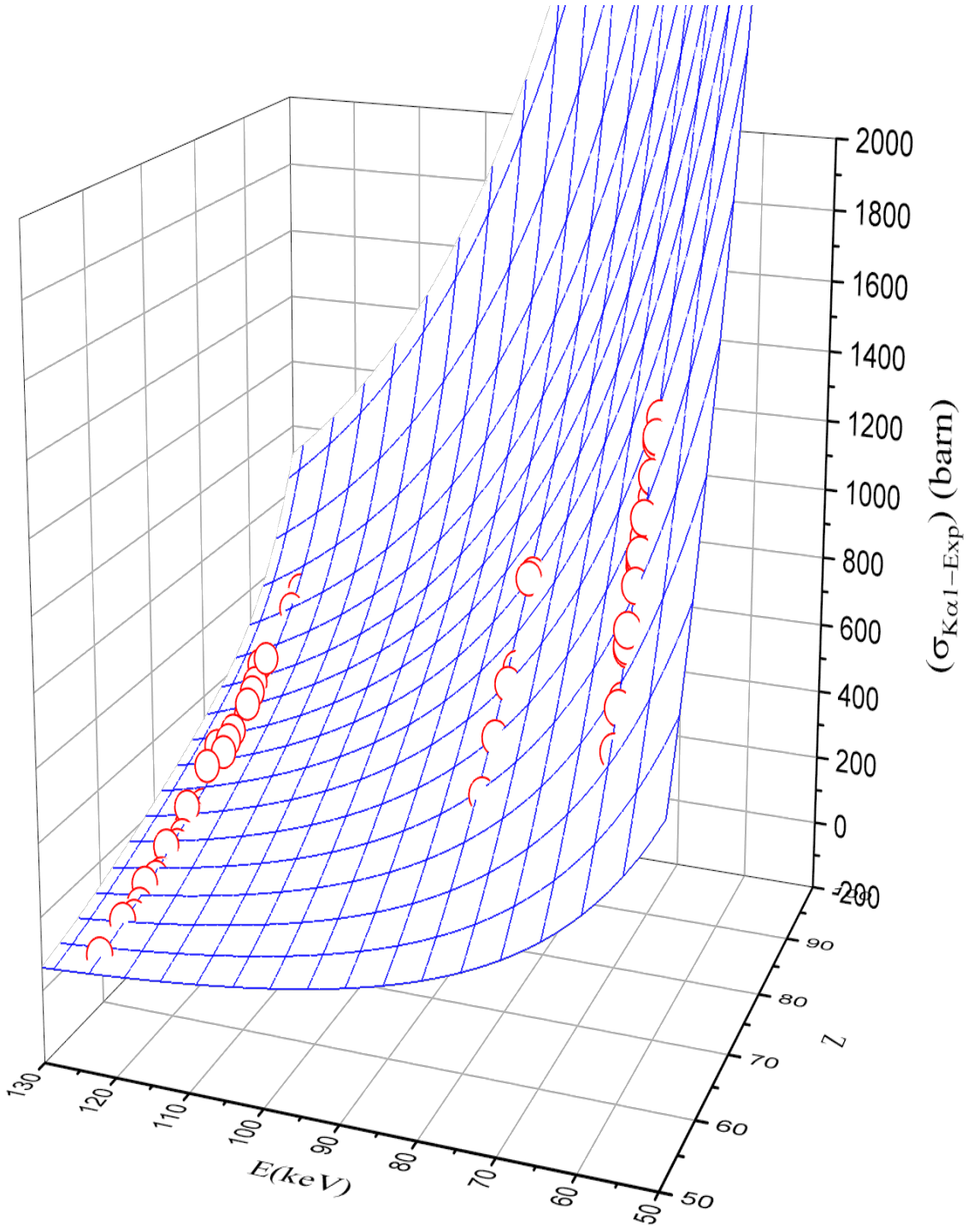
2000
1800
1600
1400
1200
1000
800
600
400
200
0
-200
$(\sigma_{K\alpha 1-Exp})$ (barn)
130
120
110
100
90
80
70
60
50
E(keV)
90
80
70
60
50
Z

Fig. 2

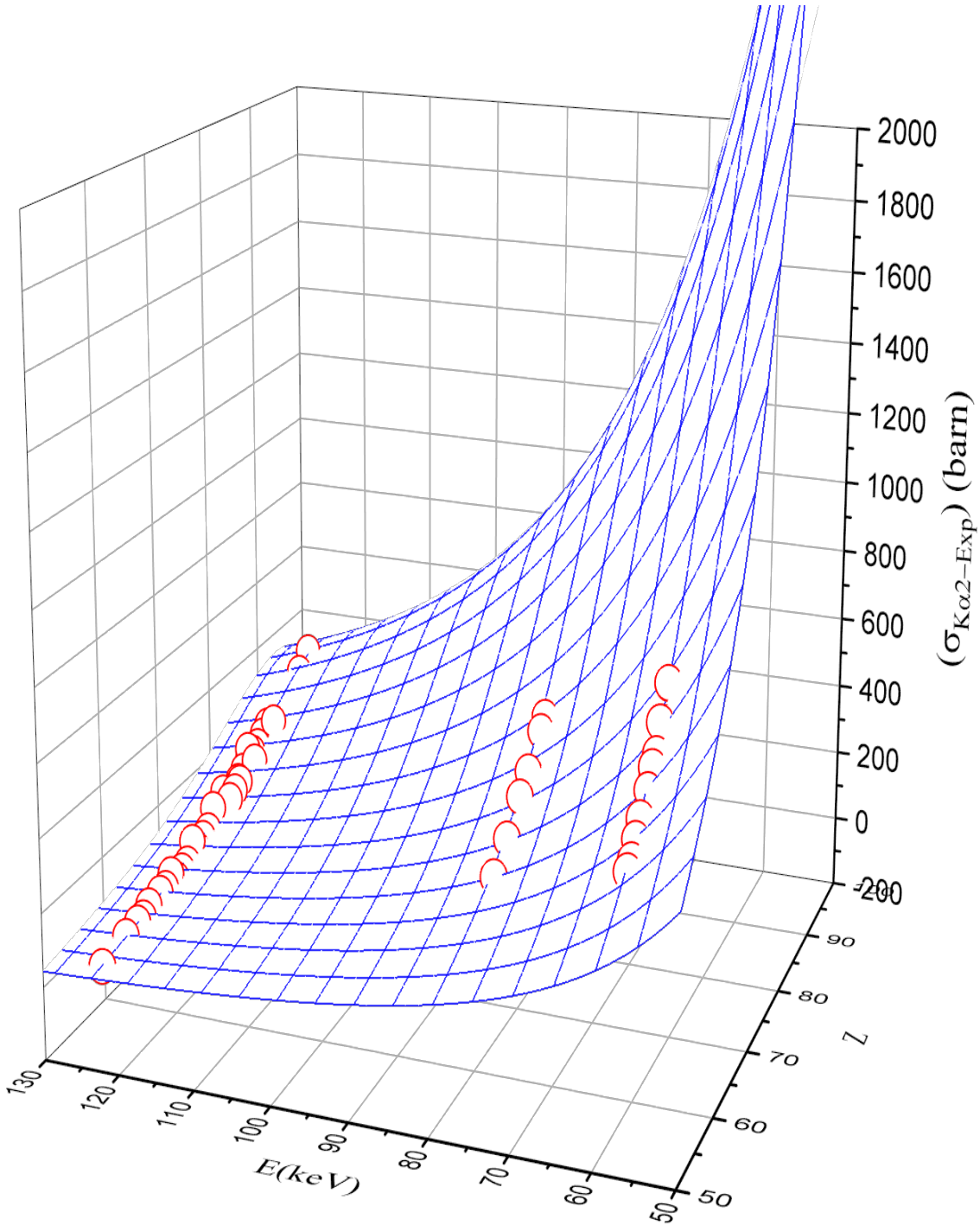
2000
1800
1600
1400
1200
1000
800
600
400
200
0
-200
$(\sigma_{K\alpha 2-Exp})$ (barn)
130
120
110
100
90
80
70
60
50
E(keV)
90
80
70
60
50
Z

Fig. 3

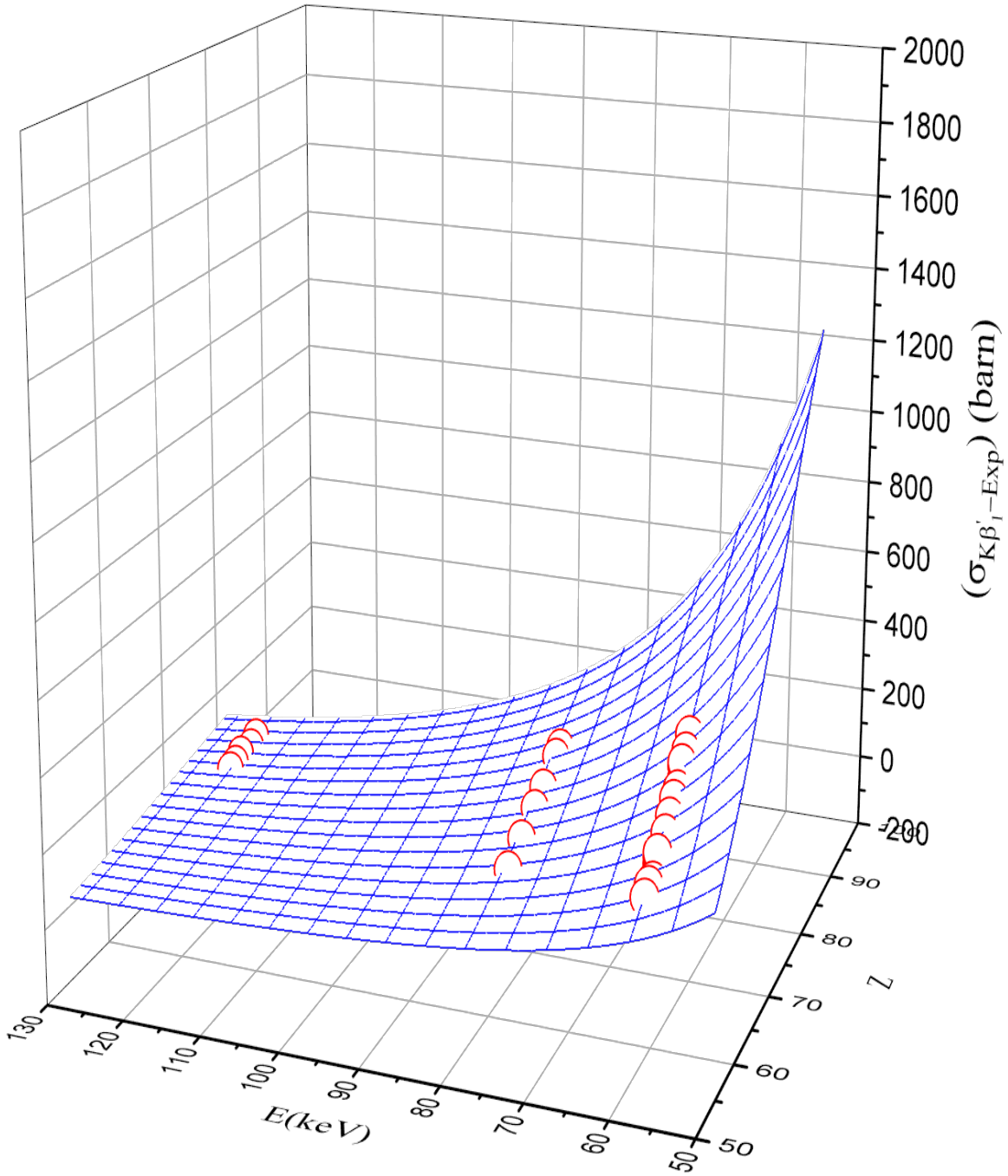
2000
1800
1600
1400
1200
1000
800
600
400
200
0
-200
$(\sigma_{K\beta'_1-Exp})$ (barn)
130
120
110
100
90
80
70
60
50
E(keV)
90
80
70
60
50
Z

Fig. 4

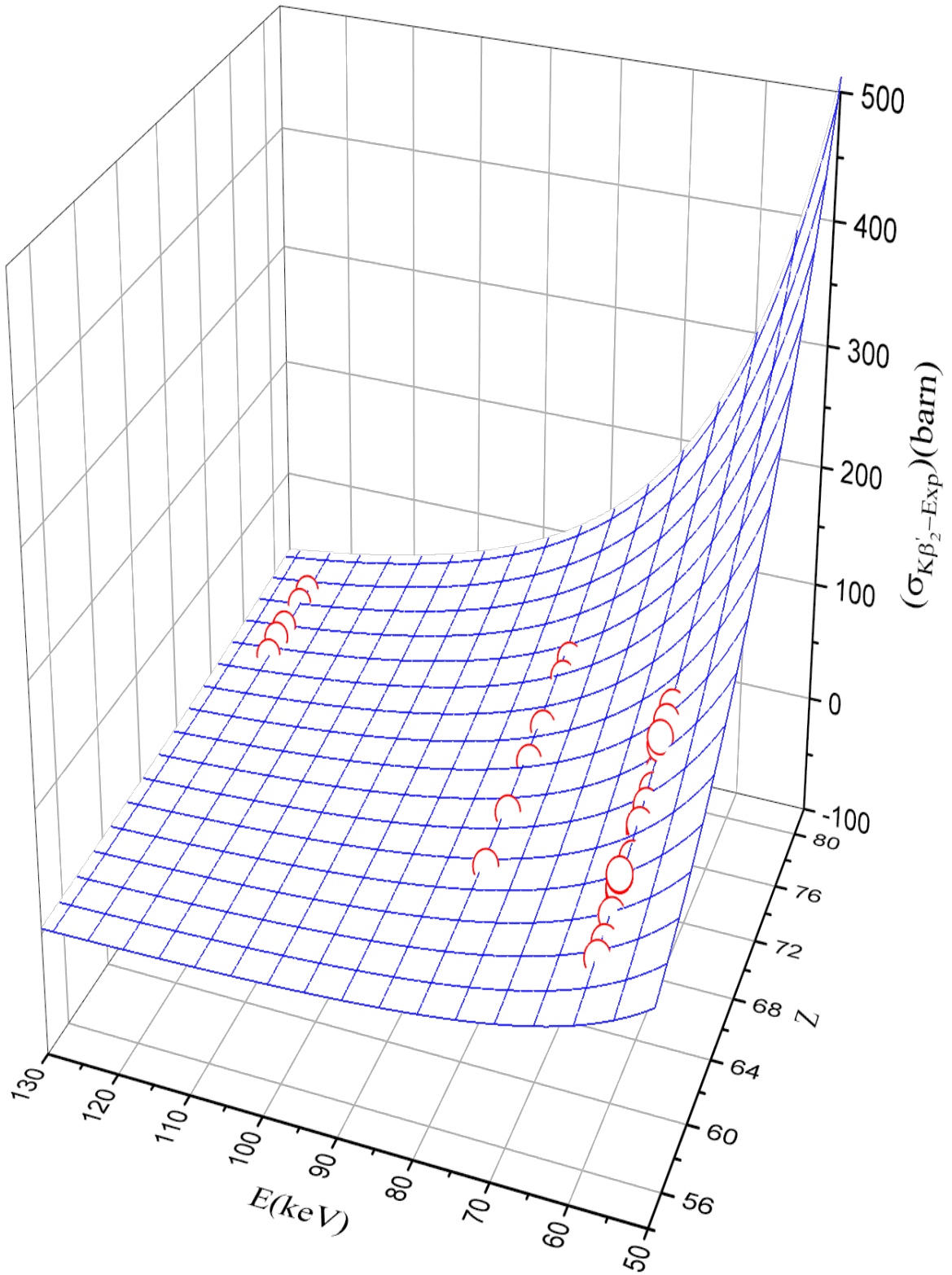
500
400
300
200
100
0
-100
$(\sigma_{K\beta'_2-Exp})$(barn)
130
120
110
100
90
80
70
60
50
E(keV)
80
76
72
68
64
60
56
Z

Fig. 5

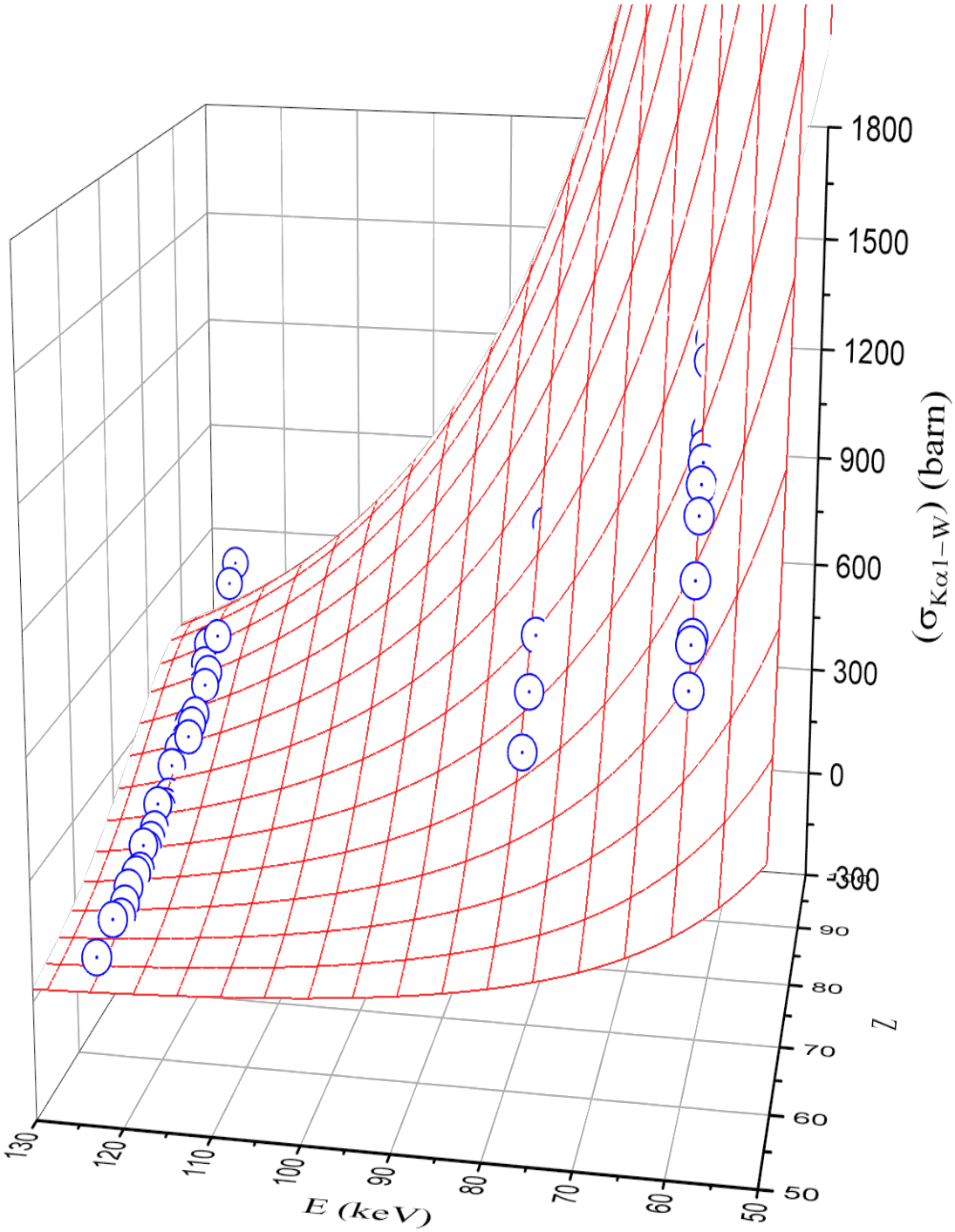
1800
1500
1200
900
600
300
0
-300
$(\sigma_{K\alpha 1-W})$ (barn)
130
120
110
100
90
80
70
60
50
E (keV)
90
80
70
60
50
Z

Fig. 6

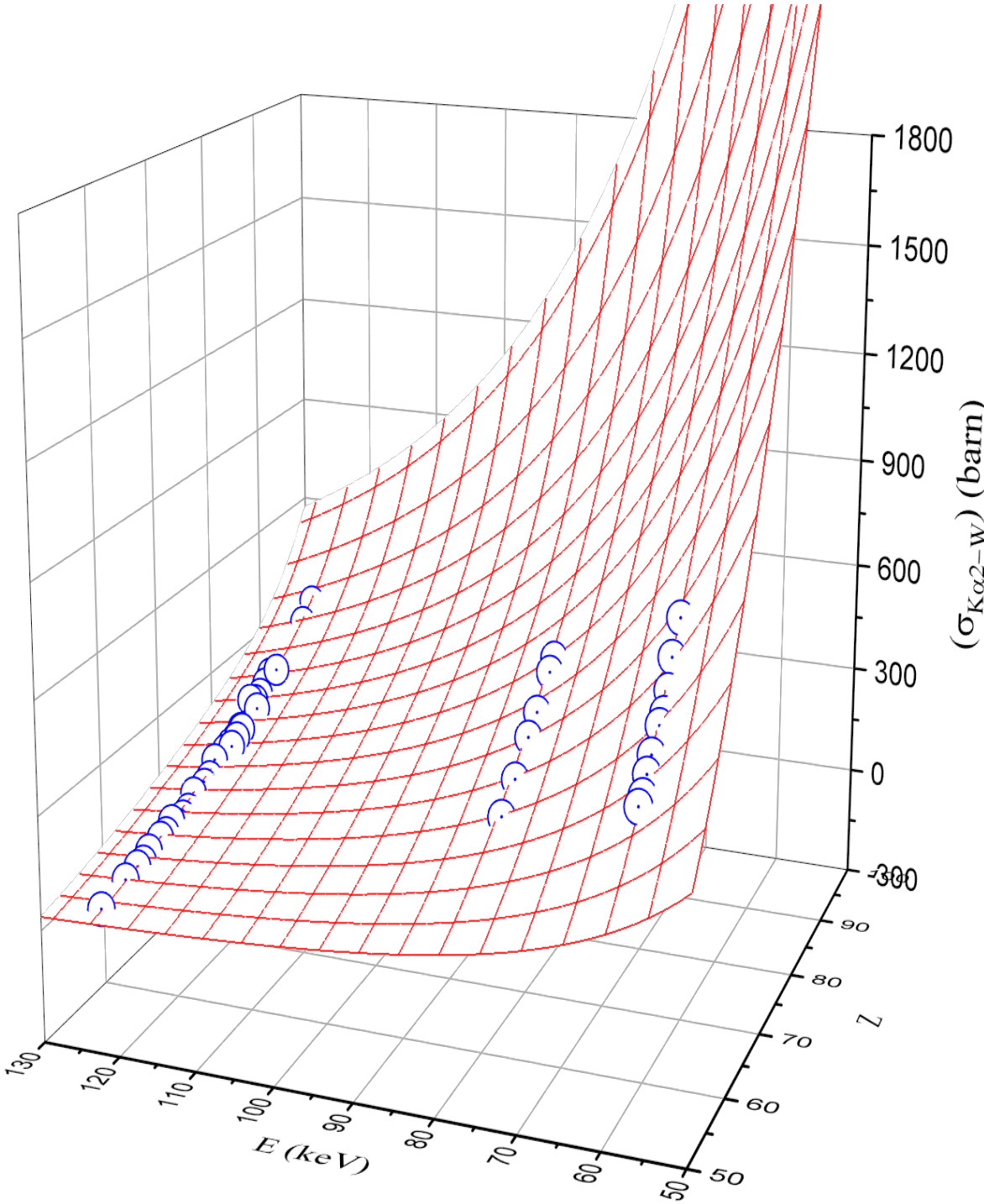
1800
1500
1200
900
600
300
0
-300
$(\sigma_{K\alpha 2-W})$ (barn)
130
120
110
100
90
80
70
60
50
E (keV)
90
80
70
60
50
Z

Fig. 7

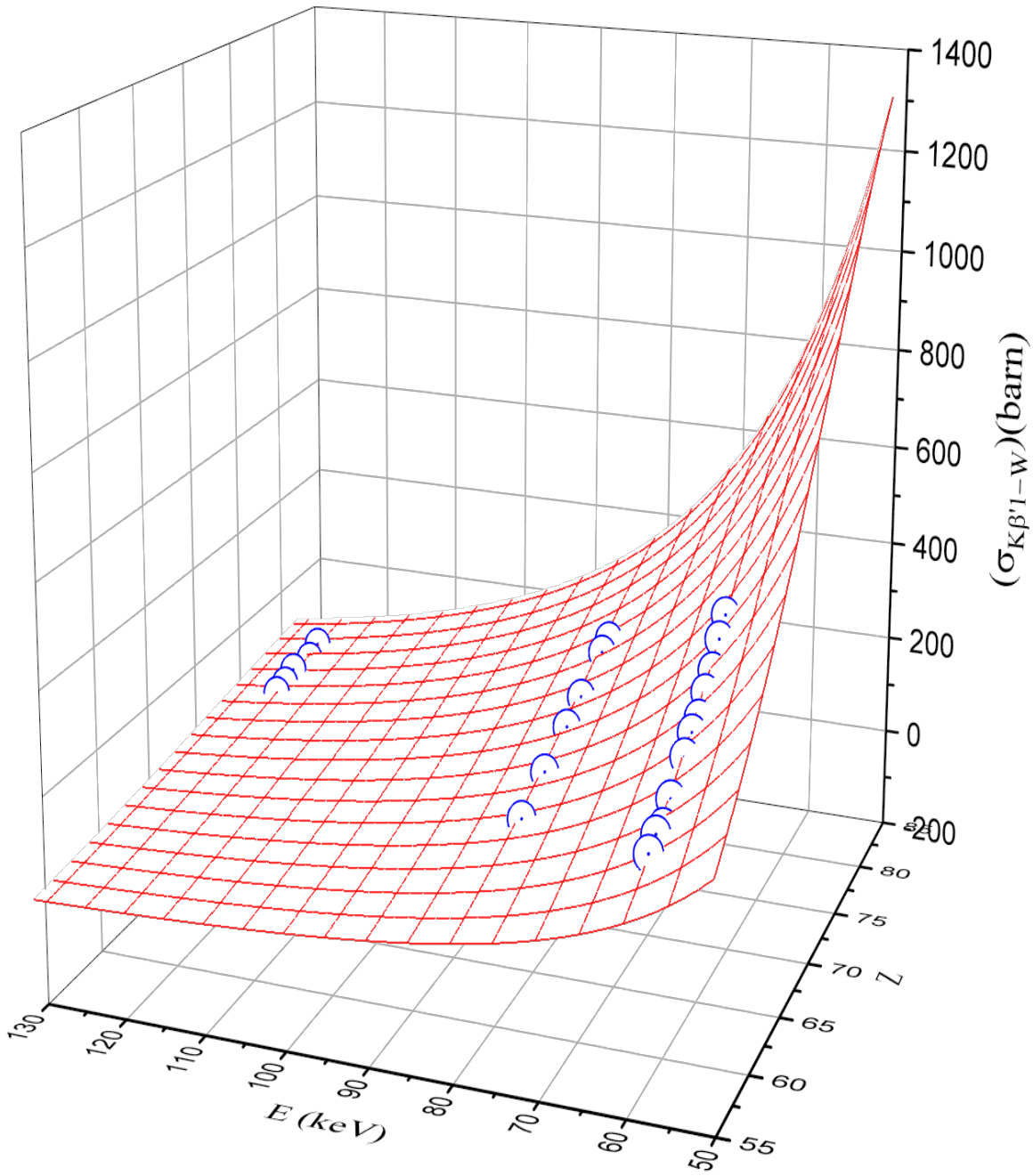
1400
1200
1000
800
600
400
200
0
-200
$(\sigma_{K\beta'1-W})$(barn)
130
120
110
100
90
80
70
60
50
E (keV)
55
60
65
70
75
80
Z

Fig. 8

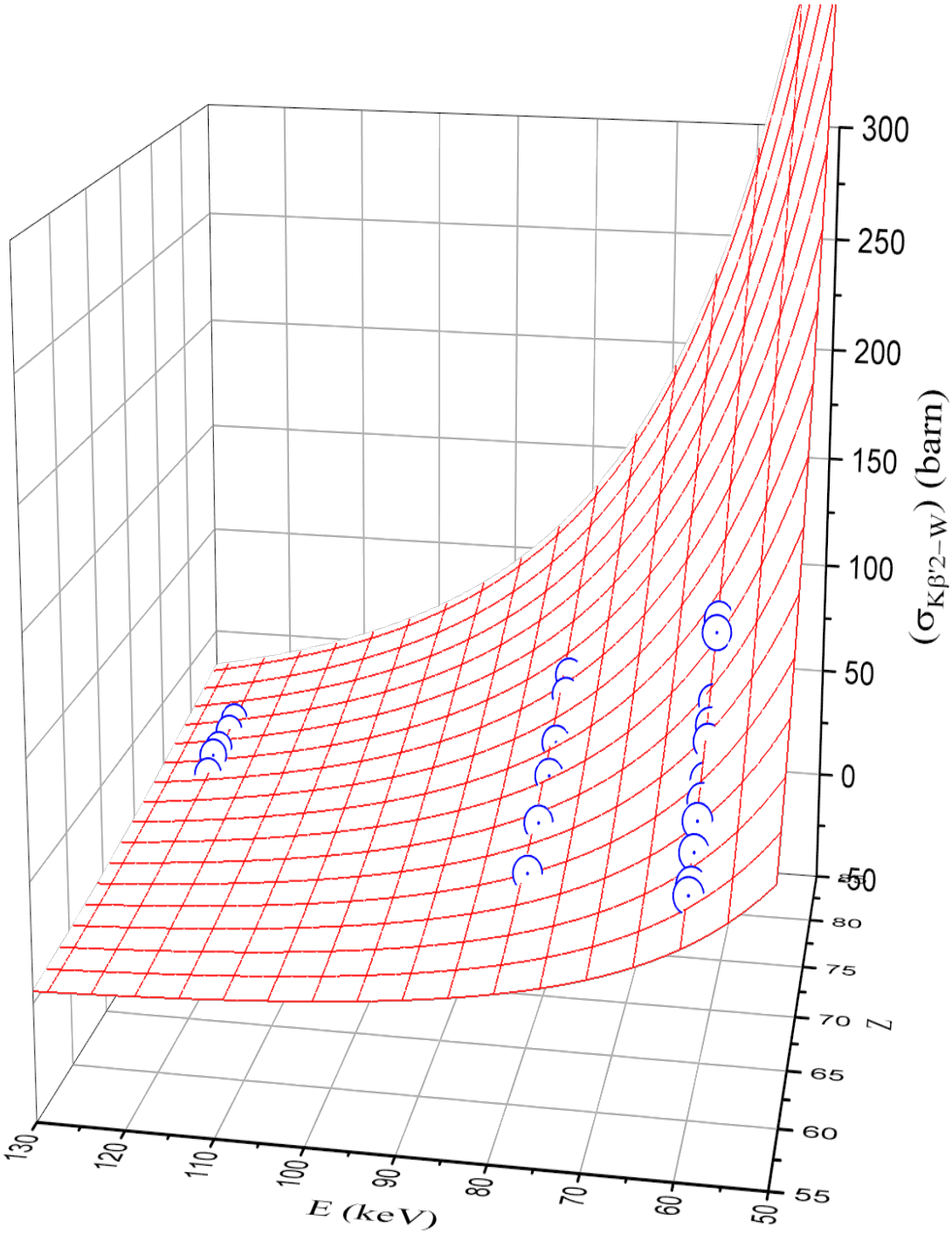
300
250
200
150
100
50
0
-50
$(\sigma_{K\beta'2-W})$ (barn)
130
120
110
100
90
80
70
60
50
E (keV)
55
60
65
70
75
80
85
Z

Fig. 9

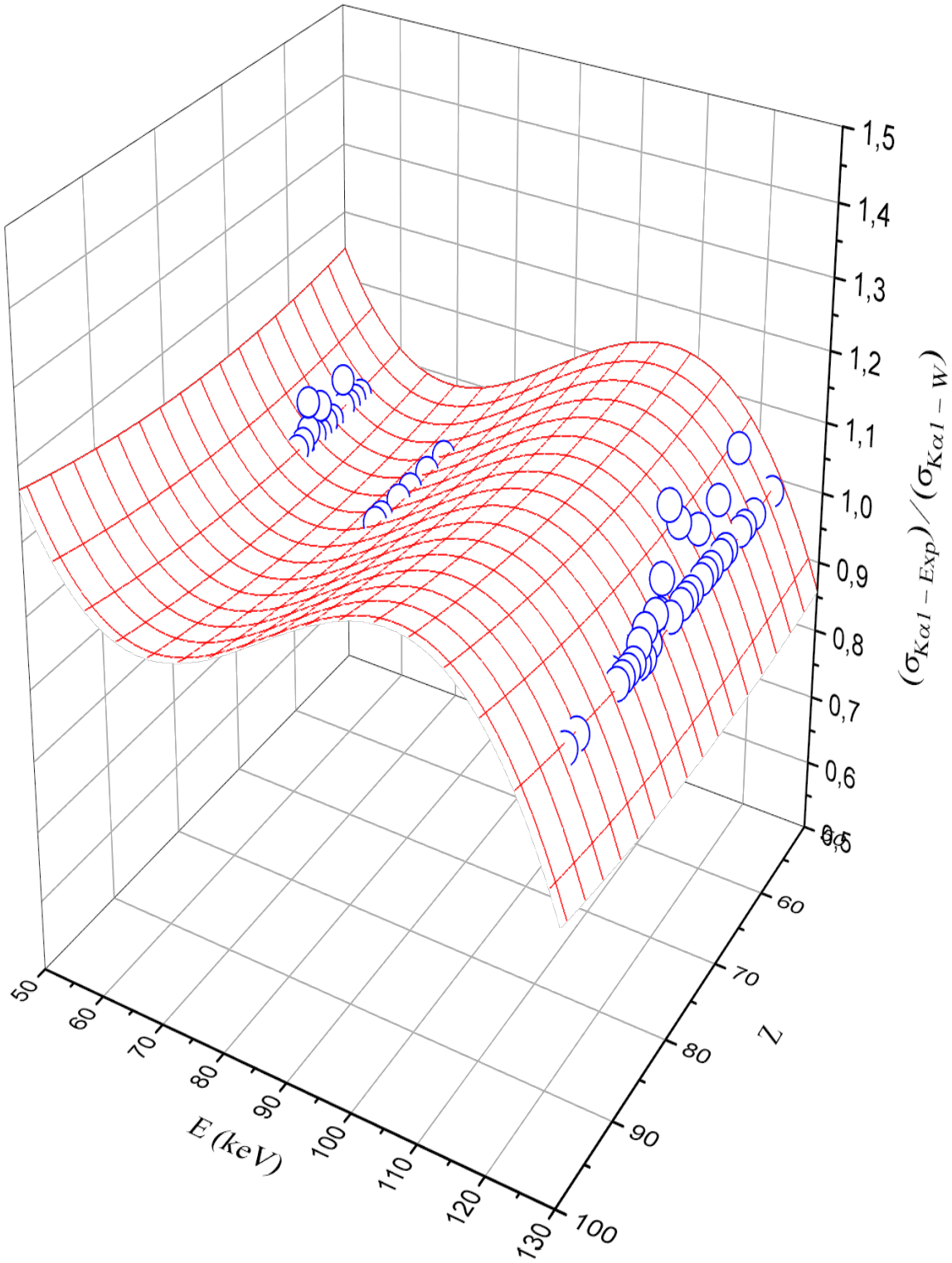
1,5
1,4
1,3
1,2
1,1
1,0
0,9
0,8
0,7
0,6
$(\sigma_{K\alpha 1-Exp})/(\sigma_{K\alpha 1-W})$
50
60
70
80
90
100
110
120
130
E (keV)
60
70
80
90
100
Z

Fig. 10

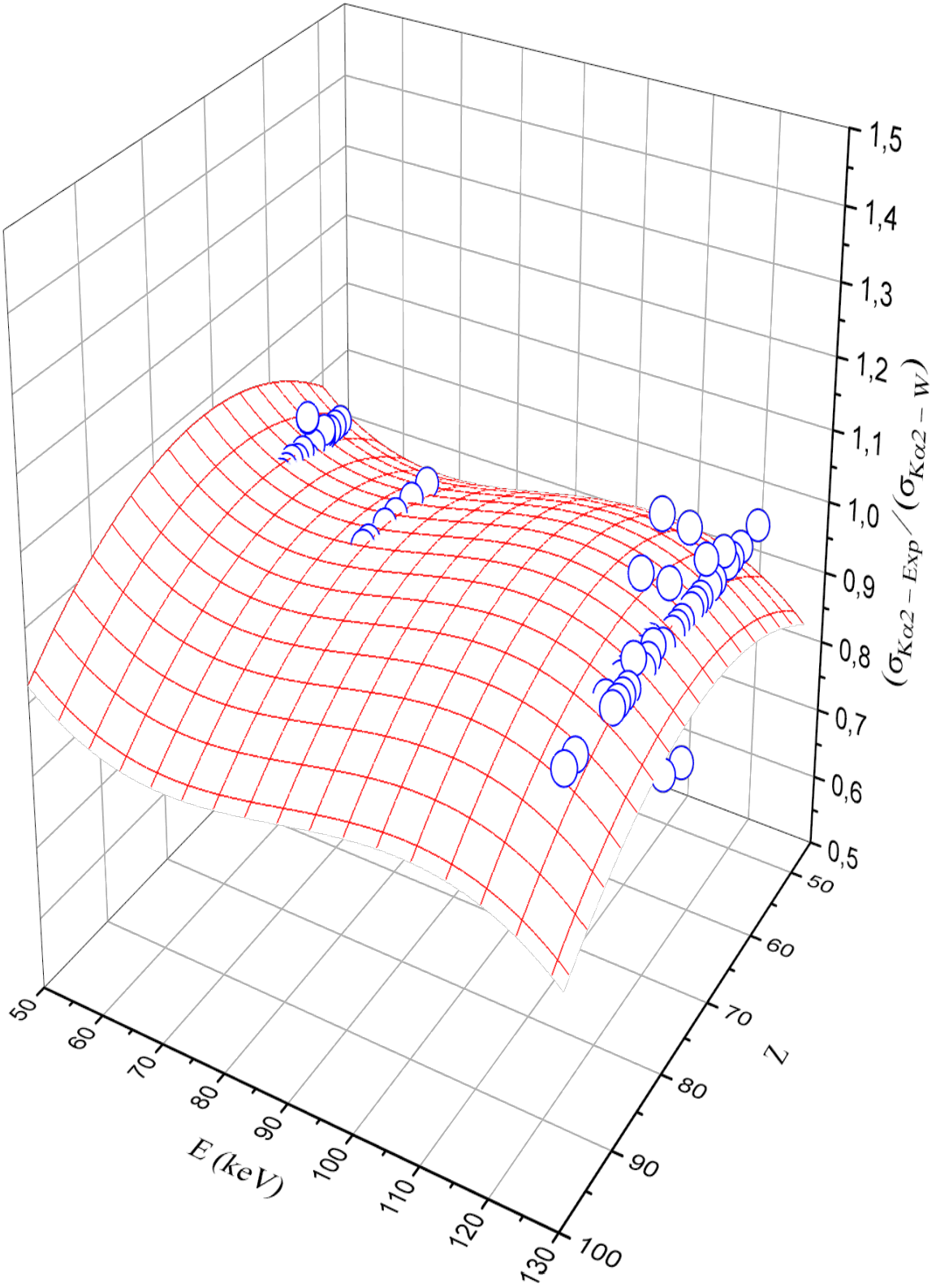
1,5
1,4
1,3
1,2
1,1
1,0
0,9
0,8
0,7
0,6
0,5
$(\sigma_{K\alpha 2-Exp}/(\sigma_{K\alpha 2-W})$
50
60
70
80
90
100
110
120
130
E (keV)
50
60
70
80
90
100
Z

Fig. 11

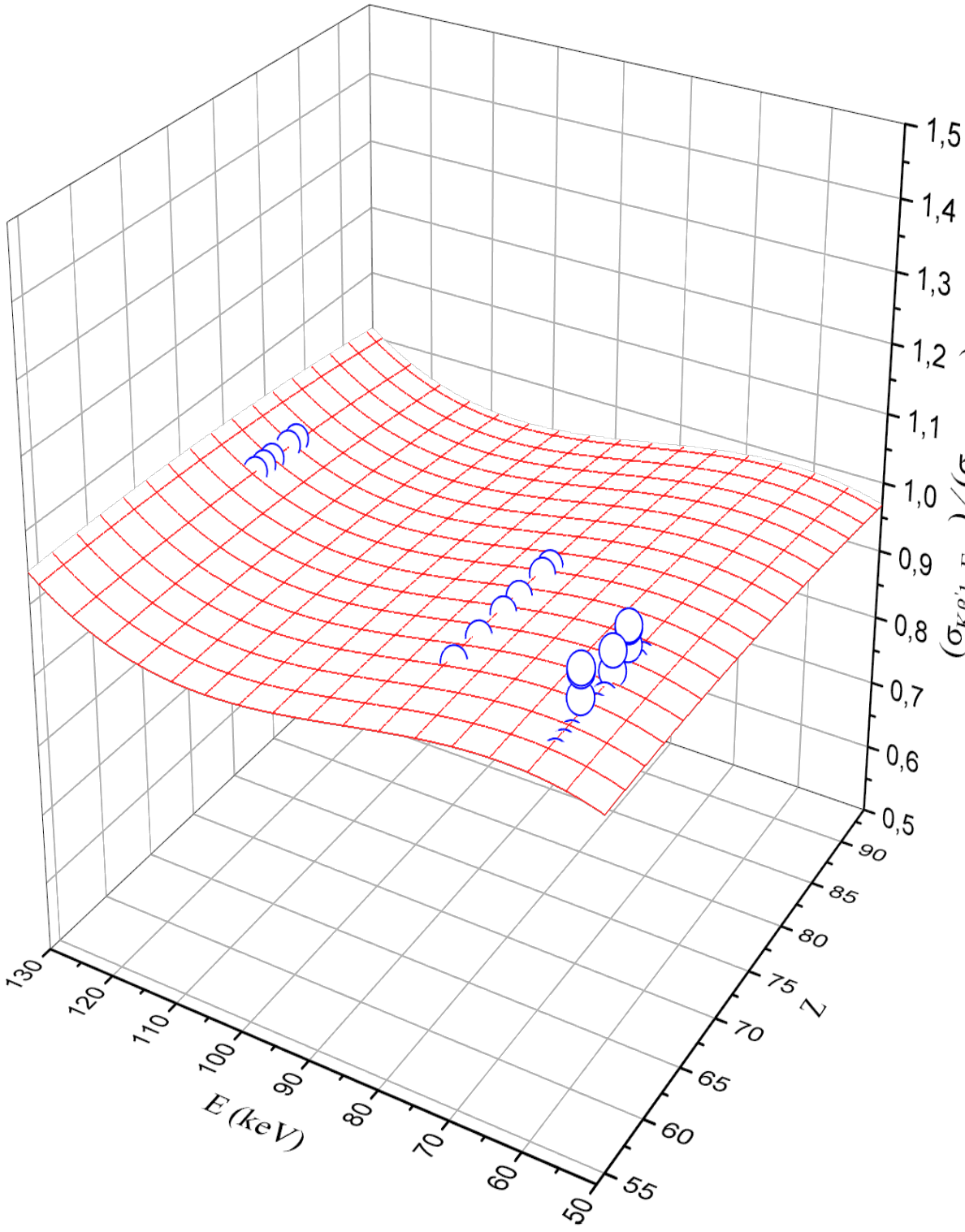
1,5
1,4
1,3
1,2
1,1
1,0
0,9
0,8
0,7
0,6
0,5
130
120
110
100
90
80
70
60
50
E (keV)
90
85
80
75
70
65
60
55
Z

Fig. 12

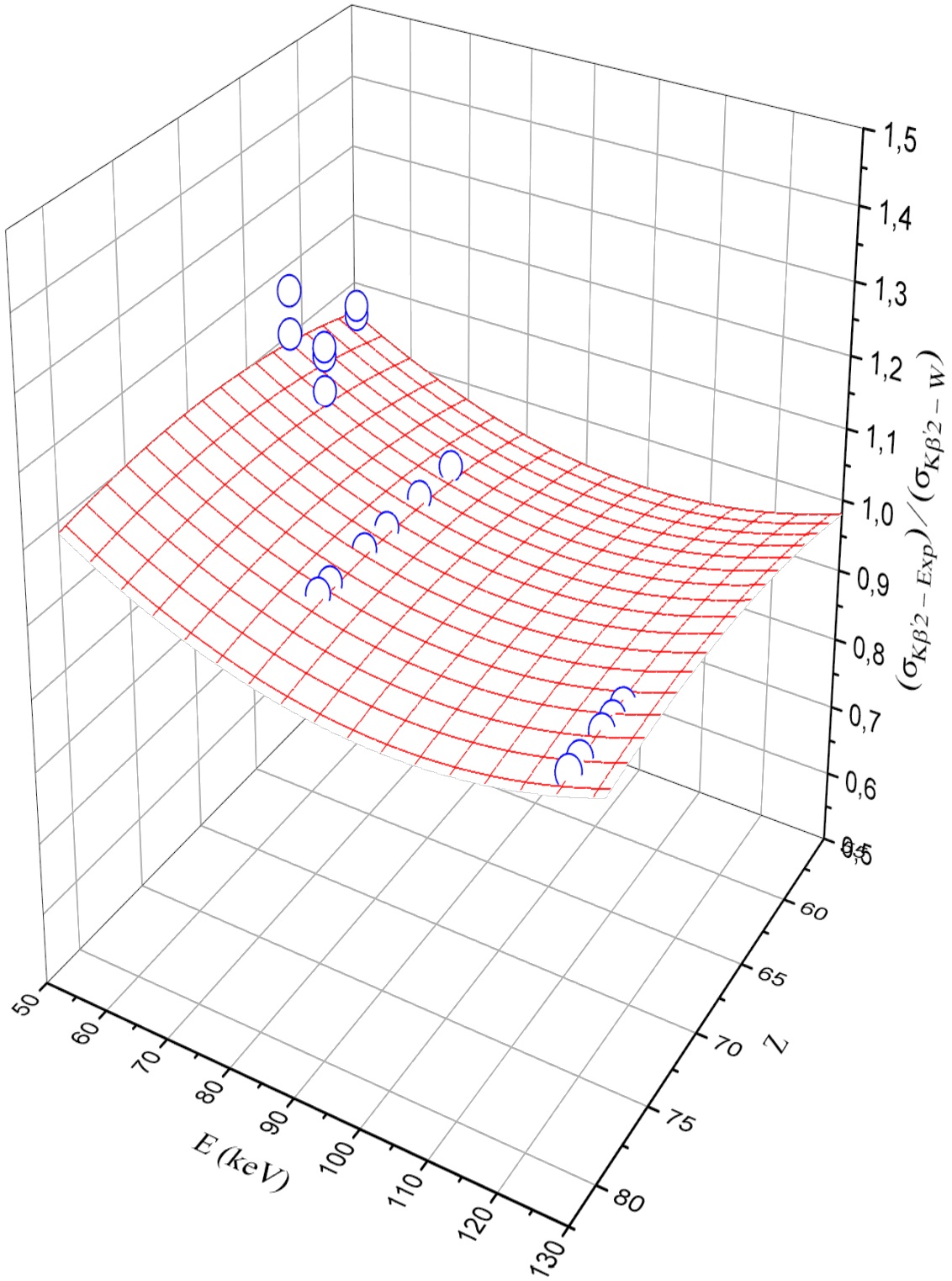
1,5
1,4
1,3
1,2
1,1
1,0
0,9
0,8
0,7
0,6
$(\sigma_{K\beta'2-Exp})/(\sigma_{K\beta'2-W})$
50
60
70
80
90
100
110
120
130
E (keV)
60
65
70
75
80
Z

Fig. 13

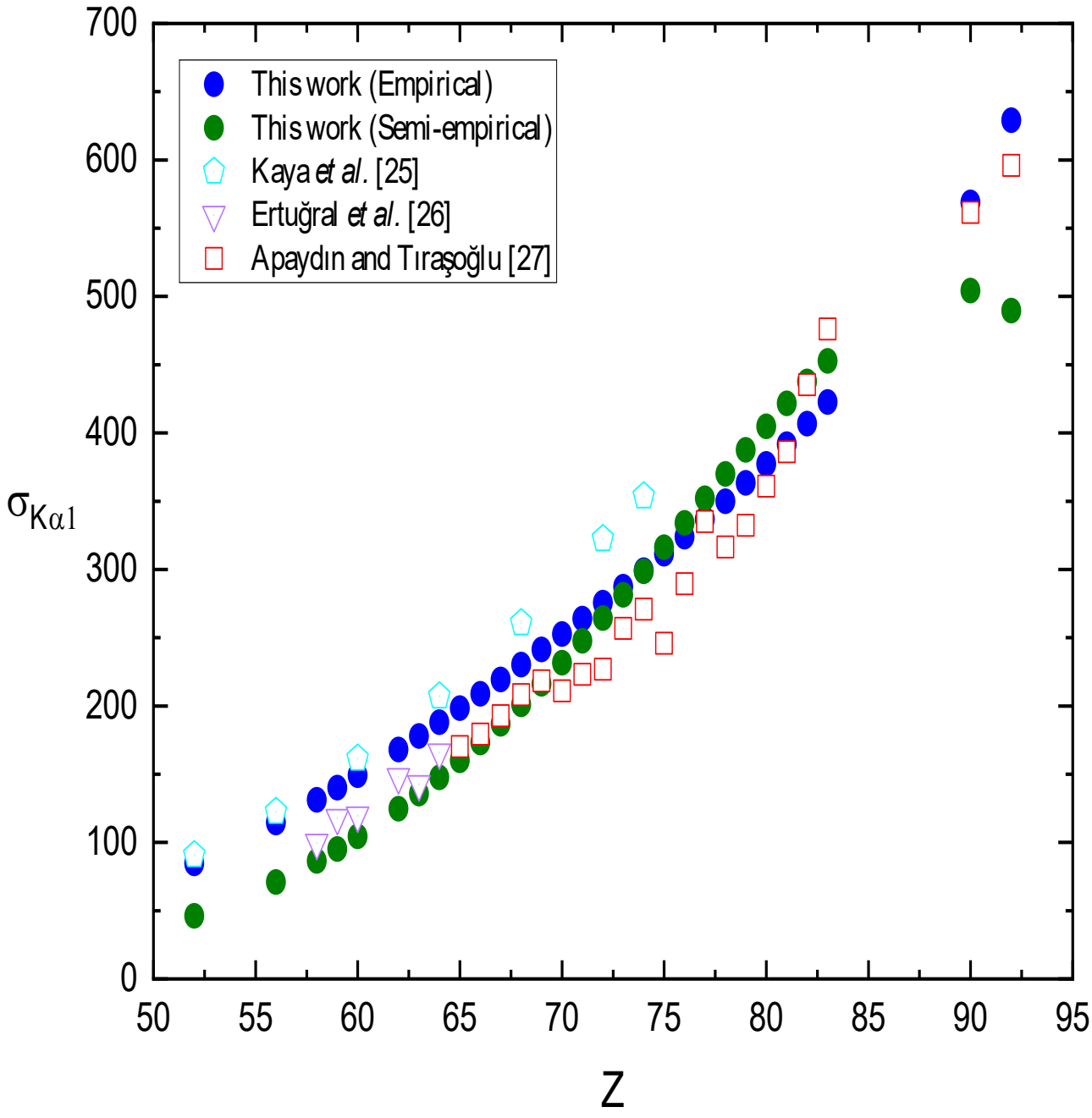
This work (Empirical)
This work (Semi-empirical)
Kaya *et al.* [25]
Ertuğral *et al.* [26]
Apaydın and Tıraşoğlu [27]
$\sigma_{K\alpha 1}$
Z
0
100
200
300
400
500
600
700
50
55
60
65
70
75
80
85
90
95

Fig. 14

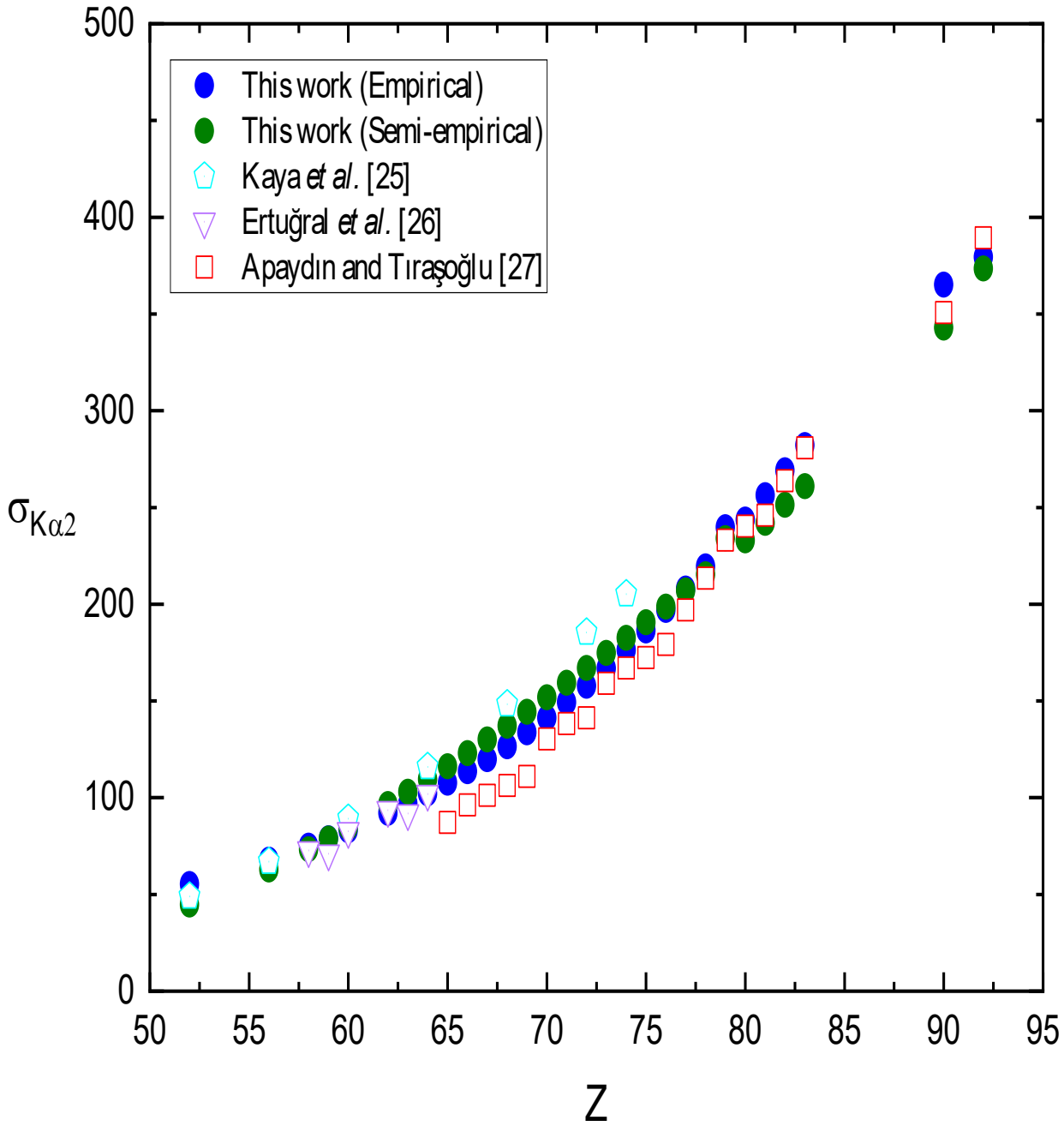
This work (Empirical)
This work (Semi-empirical)
Kaya et al. [25]
Ertuğral et al. [26]
Apaydın and Tıraşoğlu [27]
σKα2
Z
0
100
200
300
400
500
50
55
60
65
70
75
80
85
90
95

Fig. 15

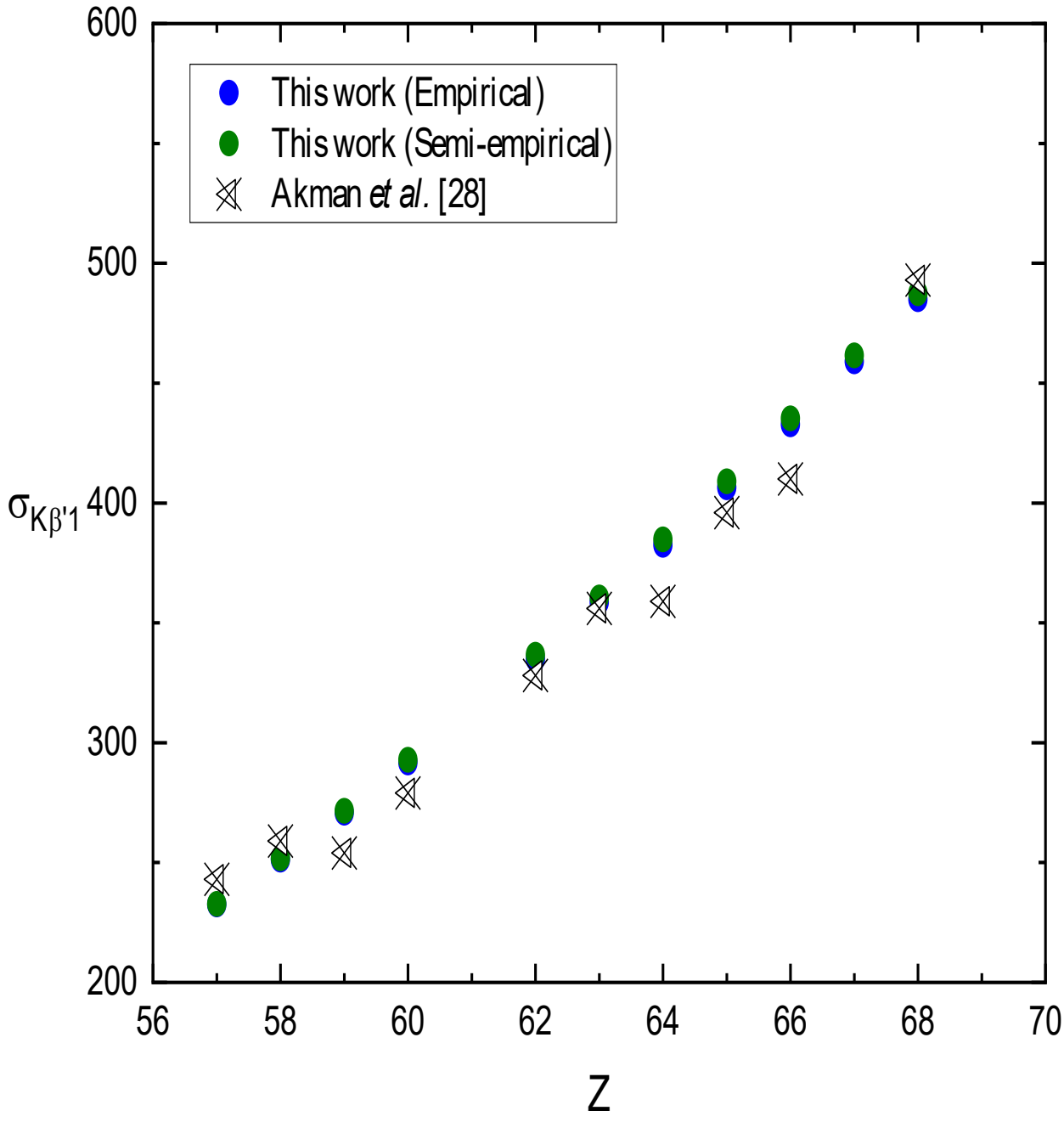
This work (Empirical)
This work (Semi-empirical)
Akman et al. [28]
σKβ'1
Z
600
500
400
300
200
56
58
60
62
64
66
68
70

Fig. 16

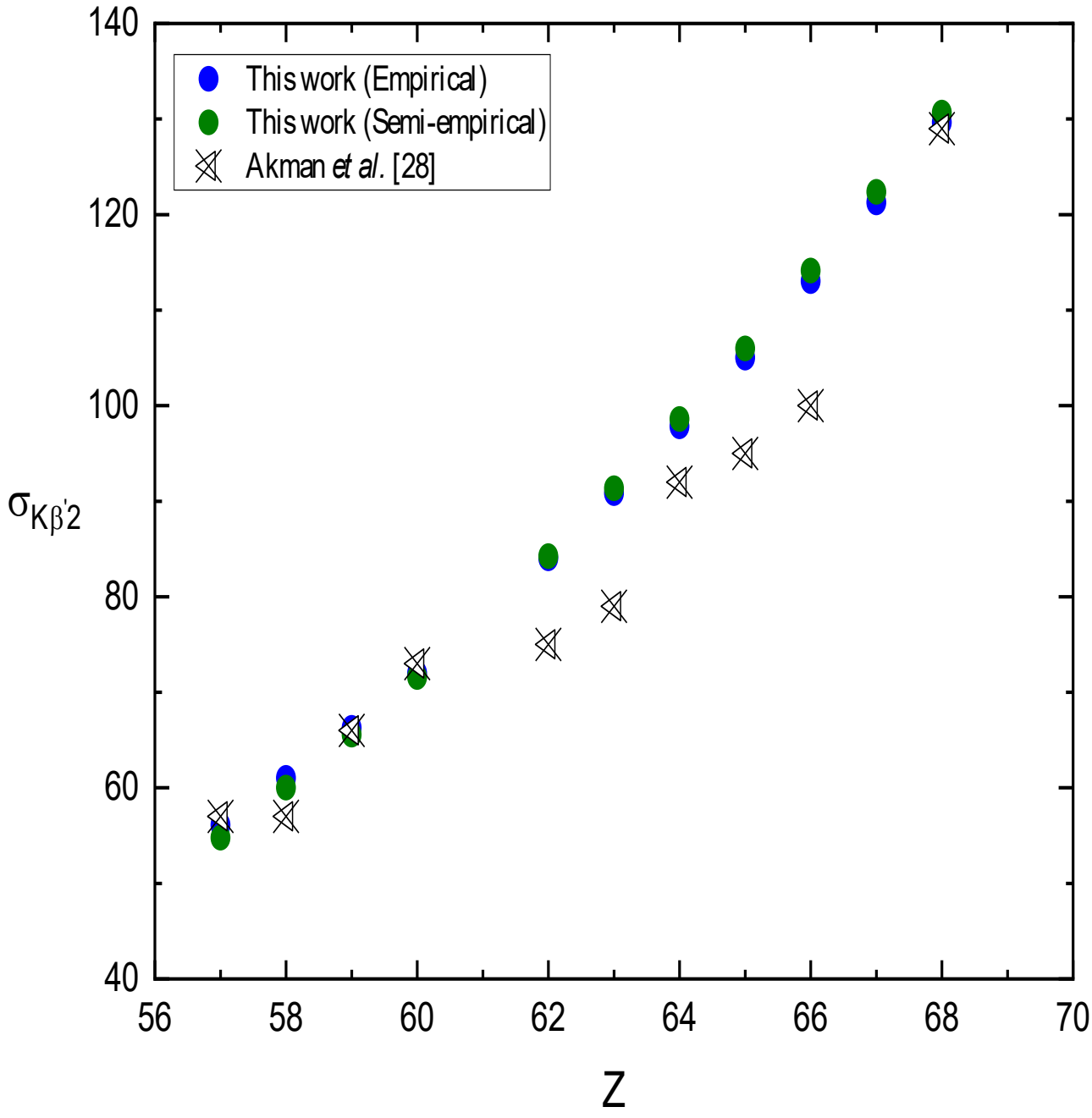
This work (Empirical)
This work (Semi-empirical)
Akman et al. [28]
σKβ'2
Z
140
120
100
80
60
40
56
58
60
62
64
66
68
70

Table 1. The fitting coefficients for the calculation of the empirical $K_{\alpha_1}, K_{\alpha_2}, K_{\beta'_1}$ and $K_{\beta'_2}$ XRF cross section for photon energy range according to the formulae (1). The associated root-mean-square errors (ε_{rms}) are also listed.

Lines	**Z-range**	**Energy (keV)**		a_i, c, d	**Values**	ε_{rms}**(%)**
K_{α_1}	$52 \leq Z \leq 92$	59.5, 78.706, 121.9 and 123.6	$P(Z)$	a_0	1509.63	10.79
				a_1	2249.3	
				a_2	-44.4708	
				a_3	0.232717	
			$g(Z,E)$	c	0.00000177436	
				d	2.57731	
K_{α_2}	$52 \leq Z \leq 92$	59.5, 78.706, 121.9 and 123.6	$P(Z)$	a_0	16474.9	8.60
				a_1	-578.904	
				a_2	7.27858	
				a_3	-0.0310159	
			$g(Z,E)$	c	0.0000191382	
				d	2.55626	
$K_{\beta'_1}$	$57 \leq Z \leq 79$	59.5, 78.706 and 123.6	$P(Z)$	a_0	1.01832	3.41
				a_1	1.38534	
				a_2	-0.0204058	
				a_3	0.0000708307	
			$g(Z,E)$	c	0.000775994	
				d	2.66562	
$K_{\beta'_2}$	$57 \leq Z \leq 79$	59.5, 78.706 and 123.6	$P(Z)$	a_0	1.01647	8.27
				a_1	1.19549	
				a_2	-0.0178464	
				a_3	0.0000793922	
			$g(Z,E)$	c	0.000672634	
				d	2.96999	

Table 2. The fitting coefficients for the calculation of the semi-empirical $K_{\alpha_1}, K_{\alpha_2}$, $K_{\beta'_1}$ and $K_{\beta'_2}$ XRF cross section for photon energy range according to the formulae (3) and (5). The associated root-mean-square errors (ε_{rms}) are also listed.

Lines	**Z-range**	**Energy (keV)**		m_n, b_i, l_j, c, d	**Values**	ε_{rms}**(%)**
K_{α_1}	$52 \le Z \le 92$	59.5, 78.706, 121.9 and 123.6	$Q(Z)$	m_0	1.00144	20.21
				m_1	1.0335	
				m_2	0.927237	
				m_3	-0.00921483	
			$H(Z,E)$	k	0.0000857379	
				γ	2.84407	
			$f(Z)$	b_0	0.105171	
				b_1	-0.000539275	
				b_2	0.00000382879	
			$R(E)$	l_0	51.8246	
				l_1	-1.50794	
				l_2	0.0181102	
				l_3	-0.0000692178	
	$52 \le Z \le 92$	59.5, 78.706, 121.9 and 123.6	$Q(Z)$	m_0	930.698	9.66
				m_1	1745.74	
				m_2	-33.7622	
				m_3	0.17489	
			$H(Z,E)$	k	0.000000746206	
				γ	2.47004	
K_{α_2}			$f(Z)$	b_0	0.000000746215	
				b_1	0.0000841906	
				b_2	-0.000000581337	
			$R(E)$	l_0	824.937	
				l_1	-17.9199	
				l_2	0.209292	
				l_3	-0.000782212	
$K_{\beta'_1}$	$57 \le Z \le 79$	59.5, 78.706 and 123.6	$Q(Z)$	m_0	1.01834	3.45
				m_1	1.38536	
				m_2	-0.0184918	
				m_3	0.0000489871	
			$H(Z,E)$	k	0.000607809	
				γ	2.62866	
			$f(Z)$	b_0	0.238544	
				b_1	0.00104733	
				b_2	-0.00000841588	
			$R(E)$	l_0	0.994966	
				l_1	0.109246	

				l_2	-0.00138369	
				l_3	0.00000548273	
$\boldsymbol{K_{\beta'_2}}$	$57 \leq Z \leq 79$	$59.5, 78.706$ and 123.6	$Q(Z)$	m_0	-0.00000841596	7.92
				m_1	478.513	
				m_2	-4.68961	
				m_3	0.00451887	
			$H(Z,E)$	k	0.000000609342	
				γ	2.78669	
			$f(Z)$	b_0	0.000000609334	
				b_1	0.000279115	
				b_2	-0.00000199044	
			$R(Z)$	l_0	151.385	
				l_1	-0.987977	
				l_2	0.00418432	
				l_3	0.00000521863	

Table 3. The empirical and semi-empirical K_{α_1} XRFCs estimated from Eq.s (1) and (8) for photo-ionization of the elements in the atomic range $52 \leq Z \leq 92$.

Element (Z)	Energy (keV)	Empirical computation	Semi-empirical computation
Te (52)	123.6	84.7	46.26
Ba (56)	123.6	114.49	70.94
La (57)	59.54	806.22	638.09
Ce (58)	59.54	862.19	703.54
	123.6	131.24	86.46
Pr (59)	59.54	920.04	773.77
	123.6	140.04	95.09
Nd (60)	59.5	981.4	850.8
	123.6	149.12	104.33
Sm (62)	59.54	1104.14	1014.47
	78.71	537.85	456.6
	123.6	168.07	124.67
Eu (63)	59.5	1170.8	1107.5
	123.6	177.9	135.8
Gd (64)	59.5	1237.05	1203.57
	123.6	187.97	147.59
Tb (65)	59.54	1302.46	1302.07
	78.71	634.45	586.04
	123.6	198.25	160.02
Dy (66)	59.5	1373.74	1411.63
	123.6	208.74	173.1
Ho (67)	59.5	1444.05	1523.52
	123.6	219.42	186.82
Er (68)	59.54	1512.97	1636.9
	78.71	736.99	736.74
	123.6	230.29	201.17
Tm (69)	123.6	241.35	216.12
Yb (70)	78.71	808.3	848.37
	123.6	252.58	231.65
Lu (71)	123.6	263.98	247.71
Hf (72)	123.6	275.57	264.27
Ta (73)	78.71	919.58	1030.08
	121.9	297.79	300.88
	123.6	287.35	281.26
W (74)	78.71	957.92	1093.65
	121.9	310.21	319.44
	123.6	299.33	298.62
Re (75)	121.9	322.86	338.32
	123.6	311.53	316.26
Os (76)	123.6	323.99	334.1
Ir (77)	123.6	336.74	352.01
Pt (78)	121.9	362.53	395.66
	123.6	349.82	369.87
Au (79)	121.9	376.5	414.56
	123.6	363.29	387.54
Ag (80)	123.6	377.23	404.85
Ti (81)	123.6	391.71	421.62
Pb (82)	121.9	421.61	468.15
	123.6	406.83	437.63

Bi (83)	123.6	422.7	452.65
Th (90)	123.6	568.92	504.21
U (92)	123.6	629.06	489.49

Table 4. The empirical and semi-empirical K_{α_2} XRFCs estimated from Eq.s (1) and (8) for photo-ionization of the elements in the atomic range $52 \leq Z \leq 92$.

Element (Z)	Energy (keV)	Empirical computation	Semi-empirical computation
Te (52)	123.6	55.28	44.75
Ba (56)	123.6	67.91	62.85
La (57)	59.54	462.14	418.27
Ce (58)	59.54	486.05	451.01
	123.6	75.13	73.26
Pr (59)	59.54	511.24	485.08
	123.6	79.02	78.79
Nd (60)	59.5	538.75	521.39
	123.6	83.13	84.54
Sm (62)	59.54	595.77	594.9
	78.71	291.92	293.97
	123.6	92.09	96.63
Eu (63)	59.5	628.51	635.04
	123.6	96.98	102.96
Gd (64)	59.5	662.23	675.19
	123.6	102.19	109.48
Tb (65)	59.54	696.91	715.1
	78.71	341.48	353.37
	123.6	107.72	116.16
Dy (66)	59.5	736.32	758.59
	123.6	113.62	123
Ho (67)	59.5	777.02	801.72
	123.6	119.9	129.99
Er (68)	59.54	818.96	844.2
	78.71	401.28	417.17
	123.6	126.59	137.13
Tm (69)	123.6	133.71	144.4
Yb (70)	78.71	447.85	461.8
	123.6	141.28	151.8
Lu (71)	123.6	149.32	159.32
Hf (72)	123.6	157.85	166.97
Ta (73)	78.71	528.99	531.55
	121.9	172.89	182.57
	123.6	166.88	174.73
W (74)	78.71	559.2	555.53
	121.9	182.76	190.81
	123.6	176.41	182.61
Re (75)	121.9	193.16	199.17
	123.6	186.44	190.61
Os (76)	123.6	196.98	198.75
Ir (77)	123.6	207.99	207.02
Pt (78)	121.9	227.38	225.13
	123.6	219.47	215.46
Au (79)	121.9	239.72	234.14
	123.6	231.38	224.07
Ag (80)	123.6	243.67	232.89
Ti (81)	123.6	256.28	241.95

Pb (82)	121.9	278.83	262.56
	123.6	269.13	251.28
Bi (83)	123.6	282.14	260.93
Th (90)	123.6	365.06	342.85
U (92)	123.6	379.42	373.54

Table 5. The empirical and semi-empirical $K_{\beta'_1}$ XRFCs estimated from Eq.s (1) and (8) for photo-ionization of the elements in the atomic range $57 \leq Z \leq 79$.

Element (Z)	Energy (keV)	Empirical computation	Semi-empirical computation
La (57)	59.54	232.5	232.72
Ce (58)	59.54	251.18	251.7
Pr (59)	59.54	270.76	271.59
Nd (60)	59.5	291.76	292.9
Sm (62)	59.54	334.84	336.6
	78.706	159.14	159.2
Eu (63)	59.5	358.57	360.59
Gd (64)	59.5	382.53	384.78
Tb (65)	59.54	193.22	193.43
	78.706	432.78	435.3
Dy (66)	59.5	432.78	435.3
Ho (67)	59.5	459	461.51
Er (68)	59.54	484.99	487.41
	78.706	230.5	230.52
Yb (70)	78.706	256.8	256.35
Ta (73)	78.706	297.73	295.78
W (74)	78.706	311.6	308.85
	123.6	93.56	94.73
Re (75)	123.6	97.74	98.69
Os (76)	123.6	101.9	102.58
Pt (78)	123.6	110.13	110.03
Au (79)	123.6	114.15	113.53

Table 6. The empirical and semi-empirical $K_{\beta'_2}$ XRFCs estimated from Eq.s (1) and (8) photo-ionization of the elements in the atomic range $57 \leq Z \leq 79$.

Element (Z)	Energy (keV)	Empirical computation	Semi-empirical computation
La (57)	59.54	56.1	54.79
Ce (58)	59.54	61.03	60.01
Pr (59)	59.54	66.28	65.56
Nd (60)	59.5	71.99	71.59
Sm (62)	59.54	84.02	84.24
	78.706	36.68	36.42
Eu (63)	59.5	90.82	91.34
Gd (64)	59.5	97.83	98.6
Tb (65)	59.54	105.03	105.98
	78.706	45.85	45.82
Dy (66)	59.5	113.04	114.13
Ho (67)	59.5	121.26	122.38
Er (68)	59.54	129.65	130.67
	78.706	56.6	56.5
Yb (70)	78.706	64.72	64.26
Ta (73)	78.706	78.47	76.71
W (74)	78.706	83.5	81.03
	123.6	21.86	23.25
Re (75)	123.6	23.23	24.51
Os (76)	123.6	24.68	25.78
Pt (78)	123.6	27.77	28.35
Au (79)	123.6	29.42	29.63